Ocean Waves Measurement and Analysis, Fifth International Symposium WAVES 2005, 3rd-7th, July, 2005. Madrid, Spain
Paper number: 88

Tsunami Landslide Generation: Modelling and Experiments

François Enet [1] and Stéphan Grilli [2], M.ASCE

Abstract: Three-dimensional fully nonlinear computations and large scale laboratory experiments are performed to investigate tsunami generation by rigid underwater landslides. Experiments were designed to ensure high repeatability of wave measurements. By varying the initial landslide submergence depth, different conditions of wave non-linearity and dispersion are generated and compared. Measured coastal runups are analyzed and found to correlate well with slide submergence depth or initial tsunami surface depression. The principle of numerical modelling, using an earlier developed model, is briefly explained. Simulations are presented and results compared to experiments. The agreement of surface elevations measured at gages with computations is quite good. Hence, the numerical model can be used to perform sensitivity analyses of generated tsunamis to landslide and slope geometric parameters, not tested in experiments.

INTRODUCTION

Underwater landslides are one of the most hazardous source of tsunamis. Since they occur mostly on the continental slope, so-called landslide tsunamis give little time to evacuate coastal populations. Moreover, while the amplitude of tsunamis generated by co-seismic displacements directly correlates with the magnitude of the earthquake, landslide tsunamis are only limited by the vertical extent of landslide motion (Murty, 1979; Watts 1998). Laboratory experiments and numerical models of tsunami generation and propagation can be used to better understand and predict tsunami hazard. Here, we present results of large scale three-dimensional laboratory experiments and, based on these, the validation of a fully non-linear potential flow model of landslide tsunami generation.

LABORATORY EXPERIMENTS

Overview

Experiments of landslide tsunami generation were carried out in the wave tank of the Department of Ocean Engineering at the University of Rhode Island (Fig. 1). In each experiment a smooth solid underwater body of Gaussian shape (truncated hyperbolic secants in both directions), made of aluminum, was located at an initial submergence depth d and

[1]Formerly at URI. Now at Alkyon, Hydraulic Consultancy & Research, PO Box 248 8300 AE Emmeloord, The Netherlands
[2]Departement of Ocean Engineering, University of Rhode Island (URI), Narragansett, RI 02882, USA

Fig. 1. Experimental set-up for landslide tsunami experiments.

Fig. 2. Example of landslide tsunami generated for $\mathrm{d} = 80$ mm.

released. The body slid on a rail, down a plane slope with $\theta = 15°$, and generated surface waves (e.g., Fig.2). The landslide body length b was 0.395 m, its width $w = 0.680$ m, and its thickness $T = 0.082$ m. The model bulk density was ρ_b = 2,435 kg/m^3. The model landslide streamlined shape was selected to reduce flow separation and allow potential flow simulations to more accurately model waves generated by the body motion.

Surface elevations were measured using capacitance wave gages placed at strategic locations (Fig. 1). The gage calibration was remotely performed during experiments using a step motors. The landslide acceleration was measured with a micro-accelerometer embedded within the body and, additionally, its displacement was recorded with an external electro-

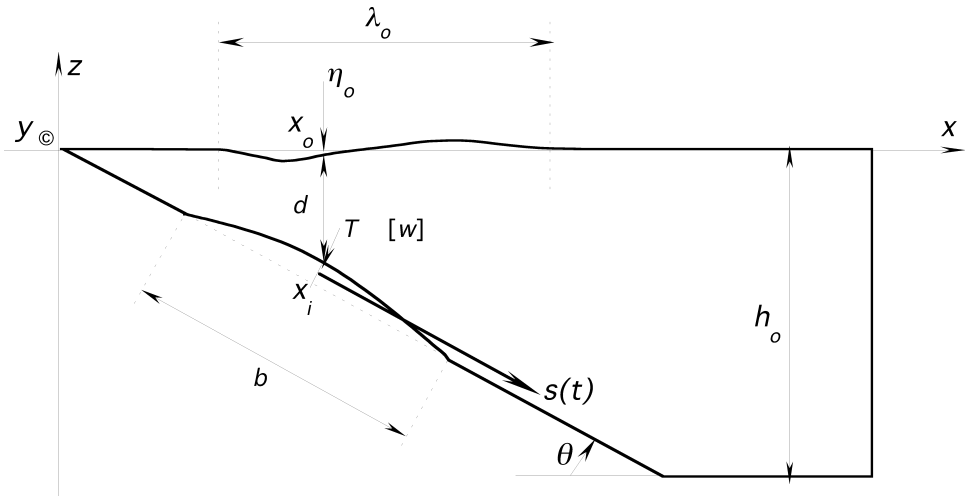

Fig. 3. Parameter definition for tsunami landslide experiments and computations.

mechanical system (gates with electric wire) at three separate locations. In each case, runup was measured on the tank axis using a video camera.

Landslide law of motion

Following the approach introduced by Grilli and Watts (2005) for both two-dimensional experiments and modeling, we describe the motion of the rigid landslide by that of its center of mass. Landslide motion and characteristic features of generated tsunamis can then be expressed as a function of six nondimensionnal independent parameters (Fig. 3): (1) a relative landslide density $\gamma = \rho_b/\rho_w$ (where ρ_w denotes water density); (2) θ; (3) the basal Coulomb friction coefficient $C_n = \tan\psi$; (4) a relative landslide submergence depth d/b; (5) a relative landslide thickness T/b; (6) and a relative landslide width w/b. Balancing inertia, gravity, buoyancy, Coulomb friction, hydrodynamic friction, and drag forces, applied on the slide, the center of mass motion parallel to the slope, $s(t)$, is governed by (upper dots denote time derivatives),

$$(M_b + \Delta M_b)\,\ddot{s} \;=\; (M_b - \rho_w V_b)(\sin\theta - C_n\cos\theta)\,g \;-\; \frac{1}{2}\rho_w\,(C_F A_w + C_D A_b)\,\dot{s}^2 \qquad (1)$$

where g is gravitational acceleration, ΔM_b, A_w, and A_b are the slide model added mass, wetted surface area, and main cross-section perpendicular to the direction of motion, respectively; C_F is a skin friction coefficient and C_D is a form drag coefficient. Eq. (1) can be integrated for landslides starting at rest, which yields,

$$s(t) = s_o\,\ln\left(\cosh\frac{t}{t_o}\right) \quad ;\text{with} \quad s_o = \frac{u_t^2}{a_o} \;;\text{and} \quad t_o = \frac{u_t}{a_o} \qquad (2)$$

the characteristic length and time of landslide motion, respectively, where,

$$a_o = g\,\sin\theta\left(1 - \frac{\tan\psi}{\tan\theta}\right)\left(\frac{\gamma - 1}{\gamma + C_m}\right) \qquad (3)$$

is the landslide initial acceleration and,

$$u_t = \sqrt{gd}\,\sqrt{\frac{b\,\sin\theta}{d}\left(1 - \frac{\tan\psi}{\tan\theta}\right)\frac{(\gamma-1)}{C_d}\,\frac{2(f^2-\varepsilon)}{f-\varepsilon}} \qquad (4)$$

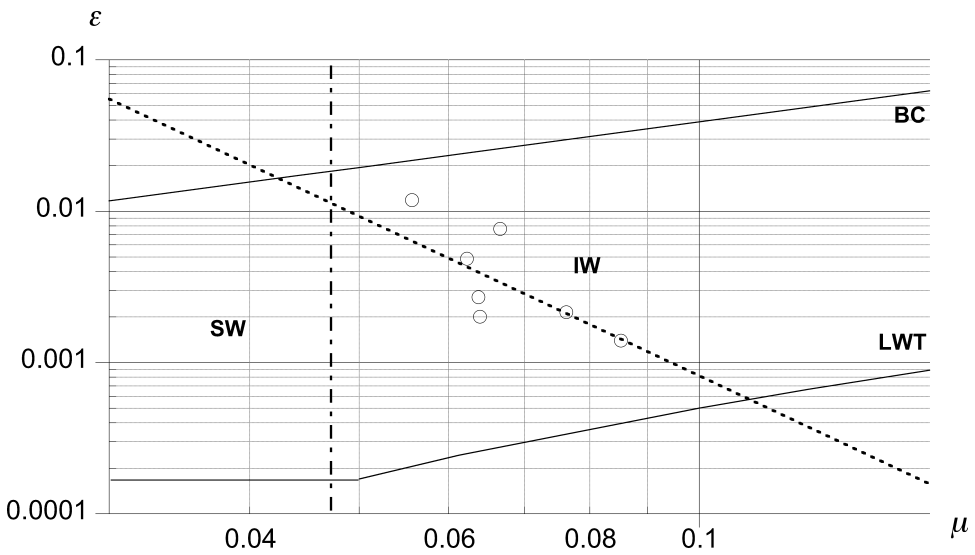

Fig. 4. Nonlinearity-dispersion space: (- - - -) theoretical relationship; (○) experimental values; BC: emprical breaking criterion; LWT: Linear Wave Theory; SW: Shallow Water waves; IW: Intermediate Water waves.

is the landslide terminal velocity. In Eq. (4), $f = 0.895$ and $\varepsilon = 0.717$ are two factors defining our landslide model shape (for further detail, see Enet and Grilli, 2005). Landslide center of mass velocity and acceleration are obtained from Eq. (2) as,

$$\dot{s} = u_t \tanh\left(\frac{t}{t_o}\right) \quad \text{and} \quad \ddot{s} = a_o \cosh^{-2}\left(\frac{t}{t_o}\right) \tag{5}$$

respectively. Based on this dimensional analysis work, one can also introduce a characteristic tsunami wavelength (Watts, 1998; Grilli and Watts, 2005; Fig. 3),

$$\lambda_o = t_o \sqrt{gd} \tag{6}$$

Experimental design

Laboratory experiments were designed to validate the numerical model by exploring an experimental space as broad as possible. All other parameters being specified as constant, the only free parameter is the initial landslide submergence d, which we vary between 61 and 189 mm (note, for measuring runup, we also vary d from -21 to 61 mm). By varying d, we can explore different conditions of nonlinearity and dispersion in terms of generated tsunami waves. Watts (1998, 2000) noted that dispersive effects in landslide tsunamis can be quantified by the parameter $\mu = d/\lambda_0$, whereas nonlinear effects can be expressed by a steepness parameter $\epsilon = a/\lambda_0$, where a is wave amplitude. Fig. 4 displays the conditions explored during experiments and shows limits for an empirical breaking criterion and the applicability of linear wave theory. As one can see, all of our cases are intermediate water waves and cover a wide range of non linearity. A theoretical relationship, based on two-dimensional (2D) computations, with three-dimensional (3D) corrections is also shown on the figure (Grilli and Watts, 2005; Watts et al., 2005; Enet and Grilli, 2005).

Repeatability

The experimental set-up was carefully designed and built to ensure a high degree of repeatability of experiments. This is illustrated in Fig. 8, which shows landslide motion and

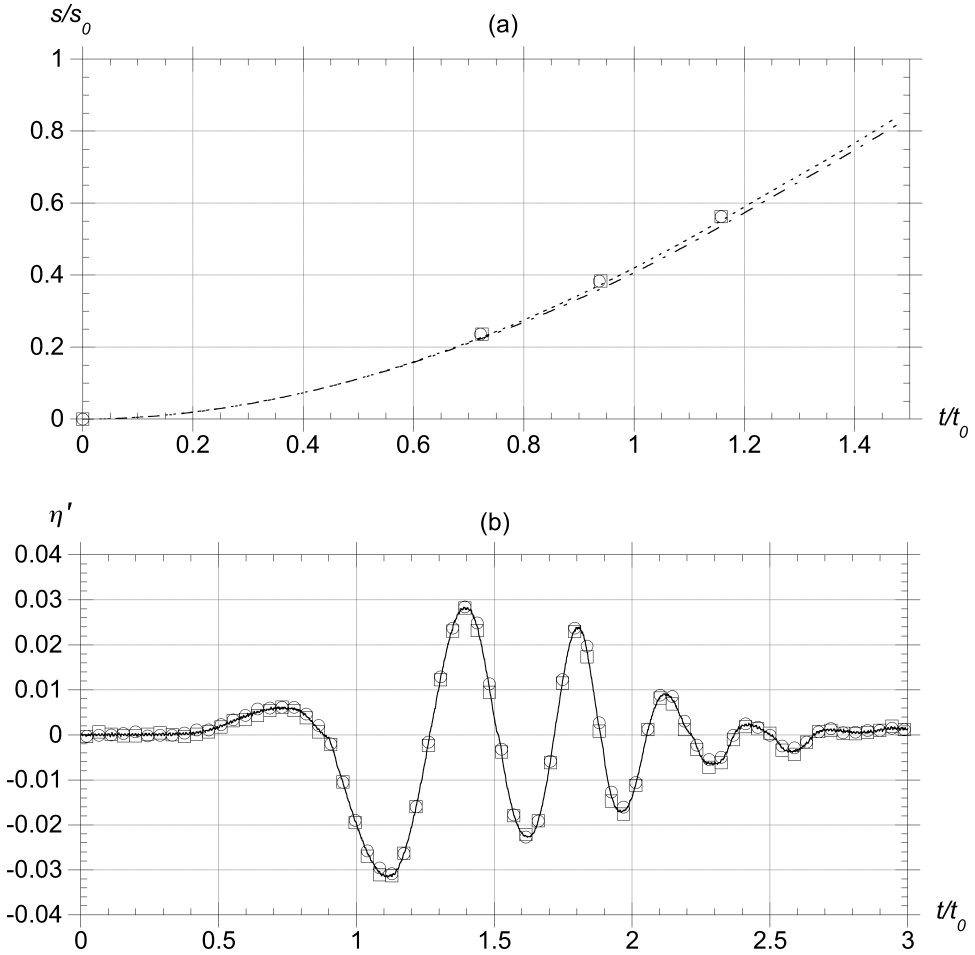

Fig. 5. Repeatability of experiments for d = 80 mm: (○) run1; (□) run 2; (—-) average. (a) Landslide motion: (- - - -) and (— - —) accelerometer; (symbols) electro-mechnical gates. (b) Wave measured at $\mathrm{x} = 1,469$ and $\mathrm{y} = 350$ mm.

free surface elevation at a gage located at $x = 1469$ and $y = 350$ mm (Fig. 3), measured for two runs with $d = 80$ mm. For motion s, accelerometer data was doubly integrated and compared to direct measurements at electro-mechanical gates. The repeatability of each model run is quite good. By averaging data measured for two such replicates of each experiment, we eliminate some of the random experimental errors. A systematic error, however, may still be part of the data.

Experimental Results

Earlier 2D work (Grilli and Watts, 2005; Watts et al., 2005) shows that the two main tsunami characteristics of interest are η_o, the maximum tsunami amplitude (usually a depression; referred to as 'characteristic amplitude') above the initial landslide position (Fig. 3), and the run-up at $y = 0$, R_u (maximum vertical inundation on the slope). Other tsunami wave characteristics can be related to η_o. Figure 6 shows values of R_u and η_o measured as a function of d ($d_{ref} = B \sin\theta = 77$ mm, is a reference depth, with $B = b\sqrt{\frac{6}{\pi}\frac{f^2-\varepsilon}{1-\varepsilon}} = 0.298$ m). Power curve fits are shown on the figures. Two regimes appear in the runup measurements in Fig. 6a, for shallow ($d/d_{ref} \leq 1$) and deep ($d/d_{ref} > 1$) initial submergence. For the shallow cases, the initial surface depression caused by the landslide motion does not

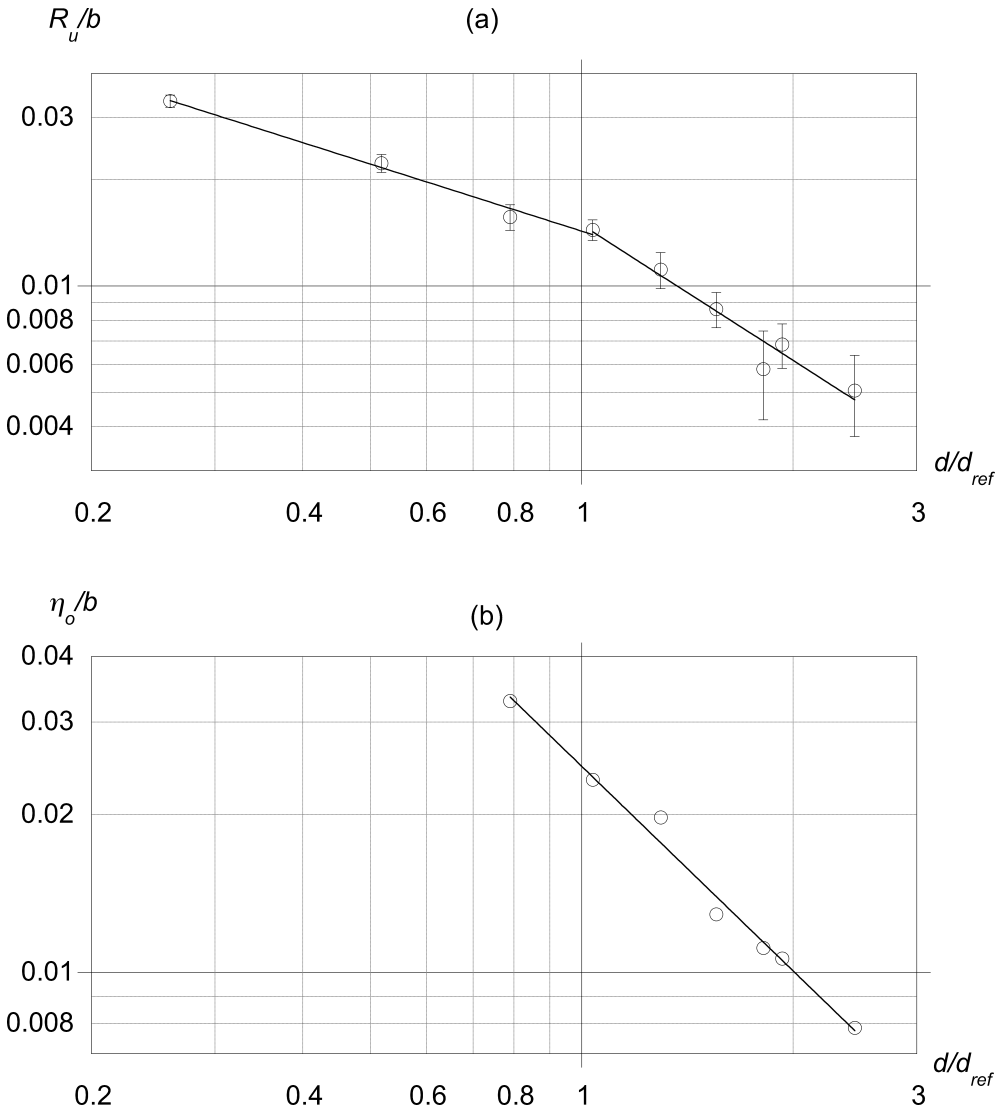

Fig. 6. Landslide tsunami runup $\mathrm{R_u}$ (a) and characteristic amplitude η_o (b), as a function of submergence depth d ($\mathrm{d_{ref}} = 0.077$ m; for runups, $\mathrm{d} = -20$ to 61 mm was added). Error bars are marked for runups. Power curve fits are shown (——).

have time to properly rebound into a large wave of elevation before the tsunami reaches the shore. Hence, for those cases, runup tends to be smaller than rundown. Some wave breaking also occurs for the shallowest submergences and emerged cases ($d < 61$ mm), which further reduces runup. This explains why runup does not grow as fast with a reduction in d in these shallower cases. Characteristic amplitudes are shown in Fig. 6b for non-breaking cases ($d \geq 61$ mm; see also Fig. 4). We find $\eta_o \propto d^{-1.29}$, i.e., an exponent quite close to "Green's law" exponent of -1.25.

NUMERICAL MODEL

We model landslide tsunamis in a 3D Numerical Wave Tank (NWT) based on Fully Nonlinear Potential Flow (FNPF) theory (Grilli et al. 2001; Grilli et al. 2002; Fochesato et al. 2005). Laplace's equation is expressed as a Boundary Integral Equation (BIE) and solved with a higher-order Boundary Element Method (BEM). A second-order explicit Lagrangian

series expansion is used for the time integration of nonlinear free surface boundary conditions. An image method is used to eliminate half the discretization of symmetrical problems with respect to axis y. A snake aborbing piston boundary is used to simulate tsunami radiation at the offshore boundary (Brandini and Grilli 2001). Governing equations are briefly summarized in the following.

Mathematical formulation

The velocity potential $\phi(\underline{x},t)$ is defined in a Cartesian referential (O,x,y,z) such that flow velocity $\underline{u} = \nabla(\phi) = (u,v,w)$. Continuity equation is Laplace's equation for the potential $\nabla^2\phi = 0$, in domain $\Omega(t)$, with boundary $\Gamma(t)$. Second Green's identity transforms this equation into the BIE,

$$\alpha(\underline{x}_l)\phi(\underline{x}_l) = \int_{\Gamma(\underline{x})} \left\{ \frac{\partial\phi}{\partial n}(\underline{x})\, G(\underline{x},\underline{x}_l) - \phi(\underline{x})\, \frac{\partial G}{\partial n}(\underline{x},\underline{x}_l) \right\} d\Gamma \tag{7}$$

with the Green's functions,

$$G(\underline{x},\underline{x}_l) = \frac{1}{4\pi r} \qquad \text{with} \qquad \frac{\partial G}{\partial n}(\underline{x},\underline{x}_l) = -\frac{1}{4\pi}\frac{\underline{r}.\underline{n}}{r^3} \tag{8}$$

and $\underline{r} = \underline{x} - \underline{x}_l$, with $r = |\underline{r}|$. We define $\alpha(\underline{x}_l) = \theta_l/4\pi$, in which θ_l is the exterior solid angle made by boundary Γ at point x_l.

Boundary conditions

Boundary Γ is divided into different parts: (i) the free surface; (ii) the slopping bottom with the moving landslide; and (iii) lateral boundaries (both solid and open). Nonlinear kinematic and dynamic boundary conditions are specified on the free surface,

$$\frac{D\underline{R}}{Dt} = \frac{\partial \underline{R}}{\partial t} + \underline{u}\cdot\underline{R} = \underline{u} = \nabla\phi \quad , \quad \frac{D\phi}{Dt} = -gz + \frac{1}{2}\nabla\phi.\nabla\phi - \frac{p_a}{\rho} \tag{9}$$

respectively, where $\underline{R}$ is the position vector of a fluid particle on the free surface, g is gravitational acceleration, ρ is fluid density, and P_a is the atmospheric pressure. A Neuman boundary condition is specified on the bottom boundary, where $\frac{\partial\phi}{\partial n}$ is obtained from the landslide law of motion. A no-flow homogenous Neuman boundary condition $\frac{\partial\phi}{\partial n} = 0$ is specified on lateral solid boundaries. These are located sufficiently far from the area of tsunami generation to have negligible effects on wave propagation. A snake absorbing boundary condition is specified on the offshore lateral boundary of Ω.

Numerical improvements

The BEM has the advantage that only boundary Γ is discretized, thus reducing the number of unknowns in the problem. The solution in the interior of the domain can then be accurately and explicitly computed as a function of the boundary solution. Weakly singular integrals, however, must be computed and the algebraic system matrix is fully populated, which yields a numerical complexity $O(N^2)$ (with N the number of discretization nodes) using an efficient iterative solver such as GMRES (which replaced the previously implemented Kaletsky direct elemination method, which was $O(N^3)$). In order to improve the efficiency of computations, a Fast Multipole Algorithm (FMA) was implemented in the spatial solver

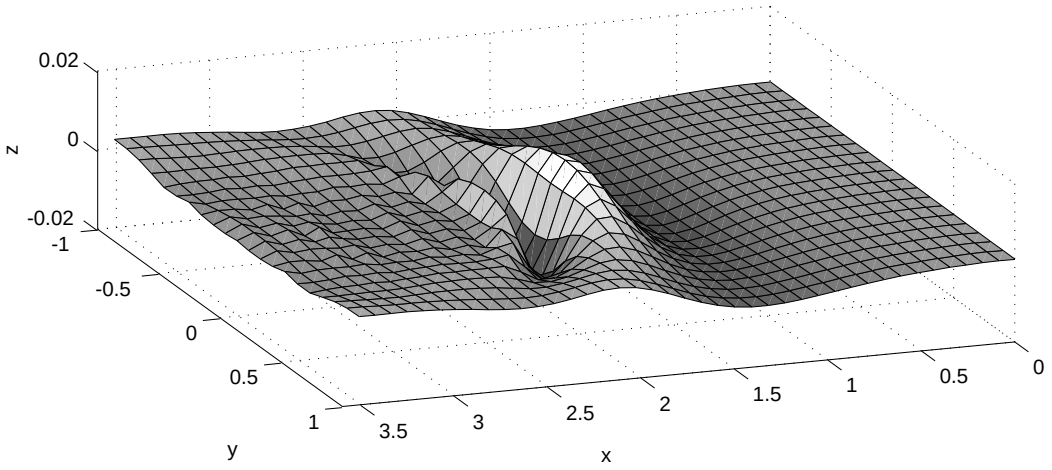

Fig. 7. Example of landslide tsunami computation for $\mathrm{d} = 80$ mm (free surface).

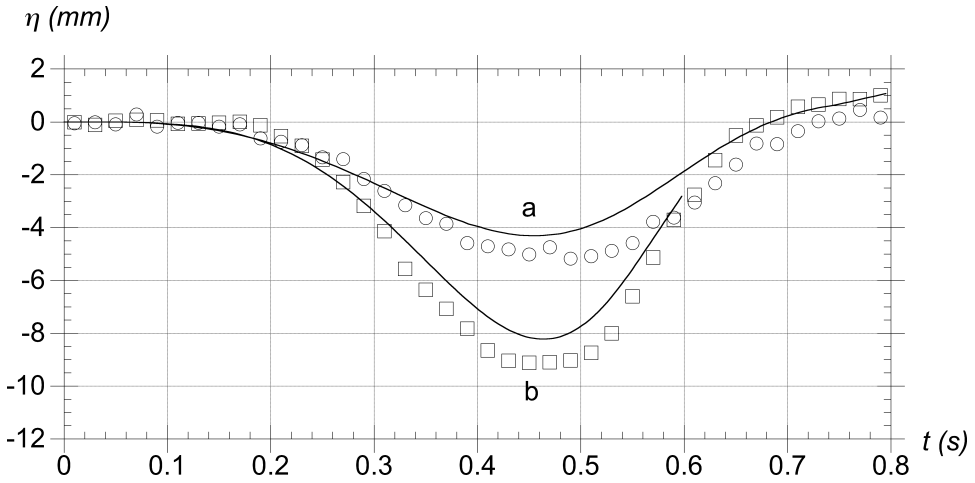

Fig. 8. Comparison of wave elevation measured at $(\mathrm{x}_0, 0)$ for $\mathrm{d} =$ a: 120 mm; b: 80 mm, with 3D numerical simulations (——).

(Fosechato and Dias, 2004) of the 3D-NWT, which theoretically can yield a $\sim O(N)$ numerical complexity for large N. Table 1 displays details of a few typical numerical cases. This powerful new FMA solver allowed us to both use larger domains and finer discretizations, and perform a convergence study of the 3D solution. We thus showed that, for quasi 2D cases (i.e., with $w/b \gg 1$), we could approach the solution of a previously validated 2D model (Grilli and Watts, 2005). The lateral image method also allowed us to roughly reduce by half the discretization size for symmetrical problems.

MODEL EXPERIMENTAL VALIDATION

The 3D-NWT was used to simulate the laboratory experiments of landslide tsunamis detailed above. Figure 7 shows a typical free surface computed for $d = 80$ mm. This is to be compared with Fig. 2. The similarity of these two figures is quite good. Model results were compared to wave measurements at gages. Figure 8 shows this comparison for $d = 80$ and 120 mm, at the gage located on the tank axis $y = 0$, at the initial location of landslide minimum submergence $x = x_o$ (Fig. 1). The maximum depression in this figure is the

Table 1. Typical computational data

Case #	Number of nodes	Spatial step Δx (m)	CPU time per time step (min)	Solver type
1	4252	0.02239	68.75	Kaletsky
2	4296	0.02361	35.98	GMRES
3	4146	0.0261	4.70	GMRES+FMA

characteristic amplitude η_o shown on Fig. 6b. The agreement between measurements and computations is quite good, with maximum absolute differences less than 1 mm, which is within the maximum estimated systematic experimental error.

CONCLUSIONS

We performed large scale laboratory experiments of tsunami generation by rigid underwater landslides. These were designed to ensure high repeatability of wave measurements. By varying the initial landslide submergence depth, different conditions of wave non-linearity and dispersion were generated and compared. Measured coastal runups were analyzed and found to vary as power functions of initial submergence depth d. The initial tsunami surface depression η_o also varies with a power function of d. Hence, we have $R_u \propto \eta_o^a$; for non-breaking cases $(d > d_{ref})$, we find $a \simeq 1$ for the tested landslide model, i.e., there is a direct one-on-one correspondence between the tsunami characteristic amplitude and coastal runup.

Three-dimensional fully nonlinear computations simulating landslide tsunami experiments were performed with an accurate and efficient NWT based on a higher-order BEM. Improvement to the NWT efficiency were made in order to solve sufficiently large and finely discretized problems. The agreement of surface elevations measured at gages with computations is quite good. Hence, the numerical model can be used to perform sensitivity analyses of generated tsunamis to landslide and slope geometric parameters, not tested in experiments. Some of these will be reported on during the conference, as well as more comparisons of numerical and experimental results for other gages, and additional submergence depths.

ACKNOWLEDGEMENTS

Support from grant CMS-0100223 from the US National Science Foundation is gratefully acknowledged. The authors are also grateful for productive discussions with and suggestions from Dr. P. Watts regarding the experimental set-up.

REFERENCES

Brandini, C. and S.T., Grilli (2001). "Modeling of freak wave generation in a 3D-NWT." In *Proc. 11th Offshore and Polar Engng. Conf.* (ISOPE01, Stavanger, Norway, 6/01), III, 124-131.

Enet, F. and Grilli, S. T. (2005). "Tsunami Generation by Rigid Underwater Landslides. Part I : Laboratory Experiments." *J. Waterway, Port, Coast, and Ocean Engineering* (to be submitted).

Fochesato, C. and F. Dias (2004). "Numerical model using the Fast Multipole Algorithm for nonlinear three-dimensional free-surface waves." (submitted)

Fochesato, C., Grilli, S. T. and Guyenne, P. (2005). "Note on non-orthogonality of local curvilinear coordinates in a three-dimensional boundary element method." *Intl J. Numer. Meth. Fluids*, 48, 305-324.

Grilli, S.T., Guyenne, P. and Dias, F. (2001). "A fully nonlinear model for three-dimensional overturning waves over arbitrary bottom." *Intl. J. Numer. Meth. in Fluids*, 35(7), 829-867.

Grilli, S. T., Vogelmann, S., and P. Watts (2002). "Development of a 3D numerical wave tank for modeling tsunami generation by underwater landslides." *Engrg. Analysis with Boundary Elements*, 26(4), 301-313.

Grilli, S. T. and Watts, P. (2005). "Tsunami generation by submarine mass failure part I : Modeling, Experimental validation, and sensivity analyses." *J. Waterway, Port, Coast, and Ocean Engineering* (accepted).

Murty, T.S. (1979). "Submarine slide-generated water-waves in Kitimat Inlet, British Columbia." *J. Geophys. Res.*, 84(C12),7,777-7,779.

Watts, P. (1998). "Wavemaker curves for tsunamis generated by underwater landslides." *J. Waterway, Port, Coast, and Ocean Engineering*, 124(3), 127-137.

Watts, P. (2000). "Tsunami features of solid block underwater landslides." *J. Wtrwy, Port, Coast, and Oc. Engrg.*, ASCE, 126(3), 144-152.

Watts, P., Grilli, S. T., Tappin, D.R. and Fryer G.J. (2005). "Tsunami generation by submarine mass failure part II : Modeling, Predictive equations and case studies." *J. Waterway, Port, Coast, and Ocean Engineering* (accepted).